

Phonon Raman scattering in $(\text{La}_{1-x}\text{Sr}_x)_2\text{CuO}_4$ single crystals

Shunji Sugai

Department of Physics, Faculty of Science, Osaka University, Machikaneyama-cho, Toyonaka 560, Japan

(Received 23 May 1988; revised manuscript received 13 December 1988)

Anomalous Raman spectra were observed in $(\text{La}_{1-x}\text{Sr}_x)_2\text{CuO}_4$ single crystals for the light polarized parallel to the layer. The number of peaks are much larger than expected from group-theoretical analysis, supposedly due to the strong phonon-magnon and phonon-free carrier interactions. With increasing x , two-phonon peaks decrease simultaneously with the decrease of the two-magnon peak; this in turn is related with the decrease of the correlation length of the antiferromagnetic spin order. Two-phonon scattering is composed of a combination of two layer-breathing modes and two layer-quadratic modes, which have strong electron-phonon interaction. A soft mode for the orthorhombic-tetragonal phase transition was found for the incident light polarized perpendicular to the layer, its energy is much higher than that observed by neutron scattering. The present Raman scattering indicates that the symmetry of the crystal with $x > 0.01$ is lower than orthorhombic.

I. INTRODUCTION

For a short time after the discovery of the superconductivity of $(\text{La}_{1-x}\text{M}_x)_2\text{CuO}_4$,¹ it was thought that the strong electron-phonon interaction of the breathing lattice vibration was the origin of the superconductivity.²⁻⁴ After a while it became obvious that the high transition temperature (T_c) of $\text{YBa}_2\text{Cu}_3\text{O}_{7-\delta}$ is hard to explain by the phonon-mediated mechanism. Also it was reported that with an increase of T_c , the isotope effect decreases in the following order: $\text{BaPb}_{1-x}\text{Bi}_x\text{O}_3$, $(\text{La}_{1-x}\text{Sr}_x)_2\text{CuO}_4$, and $\text{YBa}_2\text{Cu}_3\text{O}_{7-\delta}$.⁵⁻¹¹ With these results, the major approach turned to nonphonon mechanisms. The finding of antiferromagnetic phases in the semiconducting region of $(\text{La}_{1-x}\text{Sr}_x)_2\text{CuO}_4$ ($x < 0.01$) (Refs. 12-20) and $\text{YBa}_2\text{Cu}_3\text{O}_{7-\delta}$ ($\delta > 0.6$) (Refs. 21-23) drew much attention to the spin-fluctuation mechanism. These three-dimensional spin-ordered states compete with the superconducting states. The magnetic states in these compounds are characteristic in the respect that, even above the antiferromagnetic transition temperature T_N , spins are antiferromagnetically ordered on the two-dimensional Cu-O planes over a relatively long range as fluctuation.¹⁷ The existence of the isotope effect, however, suggests the contribution of phonon-mediated mechanisms to the superconductivity either by enhancing other mechanisms or simply contributing additively. It is useful to investigate the lattice vibrations in $(\text{La}_{1-x}\text{Sr}_x)_2\text{CuO}_4$, which has an intermediate-phonon contribution to the pairing mechanism between $\text{BaPb}_{1-x}\text{Bi}_x\text{O}_3$ and $\text{YBa}_2\text{Cu}_3\text{O}_{7-\delta}$.

Many works on Raman scattering from $(\text{La}_{1-x}\text{Sr}_x)_2\text{CuO}_4$ have been reported,^{8,18,20,24-28} but the results show lack of consistency. One of the causes of different results is the low quality of samples. Many experiments have been done on ceramics. Here the Raman studies on single crystals are presented.

The Raman spectra are different, depending on the polarization configuration of the incident and scattered light. The Raman spectra for polarization parallel to the layer show strong two-phonon scattering and two-magnon

scattering in the semiconducting region. Both scattering intensities decrease rapidly with the increase of the Sr concentration x . The two-phonon peak energies can be decomposed into combinations of two kinds of planar breathing modes and two kinds of planar quadratic modes. The large enhancement of the two-phonon peaks suggests the strong electron-phonon interaction of these modes.

The spectra with the polarization perpendicular to the layer were obtained for the first time. These spectra reveal the existence of a soft mode related to the orthorhombic-tetragonal phase transition. The energy of this mode is much higher than that measured by neutron scattering.²⁹ The assignment of the A_g modes are made on this spectra. The appearance of more peaks at $x > 0.01$ than the number expected from the reported orthorhombic structure indicates that the crystal structure is of lower symmetry.

The normal-mode analysis in the tetragonal and orthorhombic structures is made in Sec. II. The experimental procedure is described in Sec. III. The experimental results of Raman scattering are presented in Sec. IV. The assignment of the characteristic phonon modes is made in Sec. V. The discussion is given in Sec. VI, and the conclusions in Sec. VII.

II. CRYSTAL STRUCTURE AND THE NORMAL MODES

A. Crystal structure

The crystal structure of La_2CuO_4 is orthorhombic (D_{2h}^{18} , $Abma$, $CmCa$) at room temperature and tetragonal (D_{4h}^{17} , $I4/mmm$) above about 515 K.³⁰⁻³⁶ The transition temperature depends on the oxygen deficiency. The phase-transition temperature decreases with the increase of Ba or Sr concentration x .^{34,36} At $x=0.035$ the transition temperature is about 300 K. Figure 1 shows the atomic positions in the orthorhombic unit cell. This structure is formed mainly by the staggered rotation of CuO_6

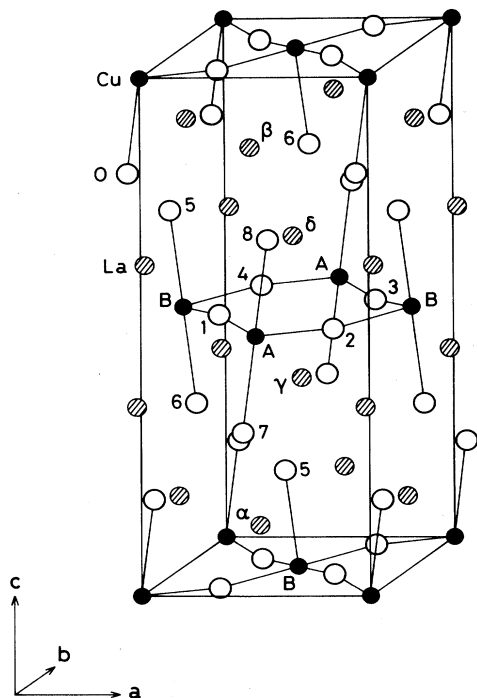


FIG. 1. Atomic positions in the orthorhombic $(\text{La}_{1-x}\text{Sr}_x)_2\text{CuO}_4$ unit cell which consists of two primitive cells. The hatched circles (α - δ) are La atoms, the filled circles (A and B) Cu atoms, and the open circles (1-8) O atoms. The rotation of CuO_6 octahedra is exaggerated.

octahedra around the axes parallel to the b axis. The crystallographic axes change from x , y , and z in the tetragonal phase into $a \parallel [110]$, $b \parallel [\bar{1}10]$, and $c \parallel [001]$. In this paper we use x , y , and z to indicate the axes in the tetragonal phase and a , b , and c to indicate the orthorhombic phase. The translational vectors for the primitive cell are $[-\frac{1}{2}, 0, \frac{1}{2}]$, $[\frac{1}{2}, 0, \frac{1}{2}]$, and $[0, 1, 0]$.

B. Normal-mode analysis

Table I lists the atomic displacements of $k \rightarrow 0$ gerade modes in the orthorhombic and tetragonal phases. Vibrations of Cu atoms make only ungerade modes. The tetragonal primitive cell includes one molecular unit and there are 12 optical modes of $2A_{1g} + 2E_g + 3A_{2u} + B_{2u} + 4E_u$,²⁴ in which the A_{1g} and E_g modes are Raman active. The A_{1g} modes are observed in the polarization configuration (x, x) , (y, y) , and (z, z) of the incident and the scattered light, and the E_g modes in (x, z) and (y, z) . In the orthorhombic phase the volume of the primitive cell is doubled with respect to the volume of the tetragonal phase and the zone-boundary modes at $(\frac{1}{2}, \frac{1}{2}, 0)$ are folded back into the Γ point. There are 39 optical modes of $5A_g + 3B_{1g} + 6B_{2g} + 4B_{3g} + 4A_u + 6B_{1u} + 4B_{2u} + 7B_{3u}$. All the gerade modes are Raman active. The A_g modes are observed in the (a, a) , (b, b) , and (c, c) polarization configurations, the B_{1g} modes in (a, b) , the B_{2g} modes in (a, c) , and the B_{3g} modes in (b, c) . The single crystal of

$(\text{La}_{1-x}\text{Sr}_x)_2\text{CuO}_4$ has twin structure, so that the exact polarization in the xy plane cannot be analyzed.

Eigenmodes are given by the linear combinations of normal modes with the same symmetry. Figure 2 shows the characteristic modes in the orthorhombic phase due to the vibrations of oxygen atoms. The A_g mode (a) corresponds to the tilting of CuO_6 octahedra around the b axis. This mode is made by the combination of the A_g^3 and A_g^4 modes. This atomic displacement is the same with that of the tetragonal-orthorhombic phase transition, so that it is expected that this mode softens toward the structural transition temperature. The (b) mode is the A_g mode due to the antiphase combination of the A_g^3 and A_g^4 modes in contrast to the (a) mode. The A_g mode (c) is the axial breathing mode in which out-of-plane O atoms vibrate symmetrically against the Cu atom. This mode is made by linear combination of the A_g^4 and A_g^5 modes. The B_{2g} modes (d) and (e) are formed by the combination of the planar breathing mode, B_{2g}^3 and B_{2g}^4 , and the symmetric vibration of out-of-plane O atoms, B_{2g}^5 and B_{2g}^6 . The B_{3g} modes (f) and (g) are the combination of the quadratic vibration of O atoms, B_{3g}^2 and B_{3g}^3 , and the vibration of out-of-plane O atoms along the b axis, B_{3g}^4 . Those vibrations which cause the change of bond length in the Cu-O plane have strong electron-phonon interactions.²⁻⁴ Espe-

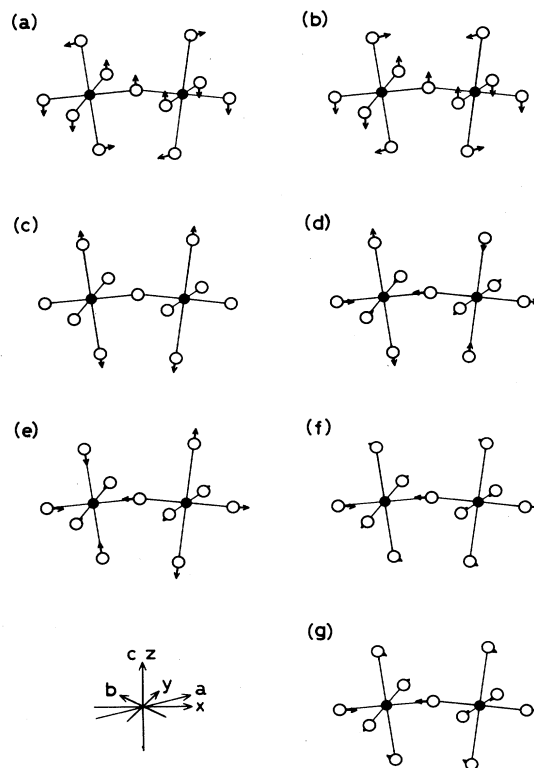


FIG. 2. Characteristic modes with oxygen atomic vibrations. (a) $A_g(c)$ mode made of $A_g^3 + A_g^4$. (b) $A_g(j)$ mode made of $A_g^3 + A_g^4$. (c) $A_g(o)$ mode made of $A_g^4 + A_g^5$. (d) $B_{2g}(u)$ mode made of $B_{2g}^3 + B_{2g}^4 + B_{2g}^5 + B_{2g}^6$. (e) $B_{2g}(v)$ mode made of $B_{2g}^3 + B_{2g}^4 + B_{2g}^5 + B_{2g}^6$. (f) $B_{3g}(p)$ mode made of $B_{3g}^2 + B_{3g}^3 + B_{3g}^4$. (g) $B_{3g}(r)$ mode made of $B_{3g}^2 + B_{3g}^3 + B_{3g}^4$.

TABLE I. Atomic displacements of $k \sim 0$ gerade modes. The listed phonon energies are for La_2CuO_4 at 30 K. The sub α - δ and 1-8 refer to the atomic positions shown in Fig. 1. The phonon energy labels correspond to those in Fig. 3.

	Orthorhombic				Phonon energy (cm^{-1})	Tetragonal
	α	β	γ	δ		
A_g^1	a	$-a$	a	$-a$	(e) 156	
A_g^2	c	$-c$	$-c$	c	(h) 229	A_{1g}^1
B_{1g}^1	b	$-b$	b	$-b$		
B_{2g}^1	a	$-a$	$-a$	a		E_g^1
B_{2g}^2	c	$-c$	c	$-c$		
B_{3g}^1	b	$-b$	$-b$	b		E_g^1
				O		
	1	2	3	4		
A_g^3	c	$-c$	$-c$	c	(j) 273 ^a	
B_{1g}^2	c	c	$-c$	$-c$		
B_{2g}^3	a	$-a$	$-a$	a		
B_{2g}^4	b	b	$-b$	$-b$		
B_{3g}^2	a	a	$-a$	$-a$		
B_{3g}^3	b	$-b$	$-b$	b		
				O		
	5	6	7	8		
A_g^4	a	$-a$	a	$-a$	(c) 126 ^b	
A_g^5	c	$-c$	$-c$	c	(o) 426	A_{1g}^2
B_{1g}^3	b	$-b$	b	$-b$		
B_{2g}^5	a	$-a$	$-a$	a		E_g^2
B_{2g}^6	c	$-c$	c	$-c$		
B_{3g}^4	b	$-b$	$-b$	b		E_g^2
Total	$5A_g + 3B_{1g} + 6B_{2g} + 4B_{3g}$					

^aCombined with A_g^4 .

^bCombined with A_g^3 .

cially the planar breathing modes have strong interaction, so that strong Raman intensity and resonant multiphonon scattering is expected.

C. Magnetic properties

The antiferromagnetic phase is observed in $(\text{La}_{1-x}\text{Sr}_x)_2\text{CuO}_4$ below T_N which depends on the oxygen deficiency. The T_N of La_2CuO_4 used in this experiment is 230 K. The T_N decreases rapidly on increasing Sr or Ba concentration to $x=0.01$.¹⁹ Two-magnon scattering is observed in the Raman spectra at about 3200 cm^{-1} for La_2CuO_4 (Refs. 18 and 20). The scattering peak rapidly decreases in intensity and shifts to lower energy, but it remains as an overdamped peak above $x=0.05$. This is presented in a separate paper.²⁰

III. EXPERIMENT

Single-phase single crystals were synthesized by a flux method using CuO . Samples with different Sr concentrations were prepared. The concentration x was determined

by electron-probe-microanalysis technique (EPMA) as $x=0$, 0.005 ± 0.001 , 0.017 ± 0.004 , 0.035 ± 0.005 , and 0.058 ± 0.004 . The antiferromagnetic transition temperature at $x=0$ is 230 K. The compounds with $x=0.035$ and 0.058 become superconducting at about 10 K. The samples used in this experiment were as-grown crystals. The surface was mechanically polished with Al_2O_3 powder. The final Al_2O_3 particle size was $0.05 \mu\text{m}$. Raman scattering was made in a backscattering configuration with the use of a double monochromator (Spex 1400) and an Ar-ion laser (Spectra Physics 164). In most of the experiments the $5145\text{-}\text{\AA}$ line was used for excitation. The laser beam of about 100 mW power was focused in an area of about $30 \times 500 \mu\text{m}^2$ of the sample surface using a cylindrical lens. All the data were corrected for the spectral efficiency of the spectrometer and the photomultiplier using a standard lamp. The samples were set in a He-gas-flow cryostat for the low-temperature measurement and in a furnace for the high-temperature measurement. The atmosphere around the sample was He for the measurement in the cryostat, while air was present in the furnace in order to avoid the decrease of oxygen concentration at higher temperatures.

IV. EXPERIMENTAL RESULTS

A. $(x, x+y)$ spectra

Figure 3 shows the $(x, x+y)$ Raman spectra in $(\text{La}_{1-x}\text{Sr}_x)_2\text{CuO}_4$ with $x=0, 0.005 \pm 0.001, 0.017 \pm 0.004, 0.035 \pm 0.005$, and 0.058 ± 0.004 at 30 K. The polarization of the incident light is parallel to the x axis. The scattered light polarization is not analyzed, but the (x, x) component is dominant. All of these samples are in the orthorhombic phase at this temperature. In this polarization configuration the A_g and B_{1g} modes are observable for the reported orthorhombic structure. Most of the sharp peaks below 800 cm^{-1} are one-phonon process peaks and the peaks between 800 and 1500 cm^{-1} are two-phonon process peaks. The spectra in $(\text{La}_{1-x}\text{Sr}_x)_2\text{CuO}_4$ with small x are in the resonant scattering condition for visible light. The number of peaks below 800 cm^{-1} is much larger than that of the allowed phonon modes, $5A_g + 3B_{1g}$. As discussed later some mechanism makes the forbidden modes, B_{2g} and B_{3g} , active.

The intensities of the resonant two-phonon peaks at $800\text{--}1500 \text{ cm}^{-1}$ decrease with the increase of x and they almost disappear above $x=0.035$ together with the simultaneous extinction of the two-magnon peak. Even in single-phonon peaks below 800 cm^{-1} drastic change is observed for the Sr concentration above or below about

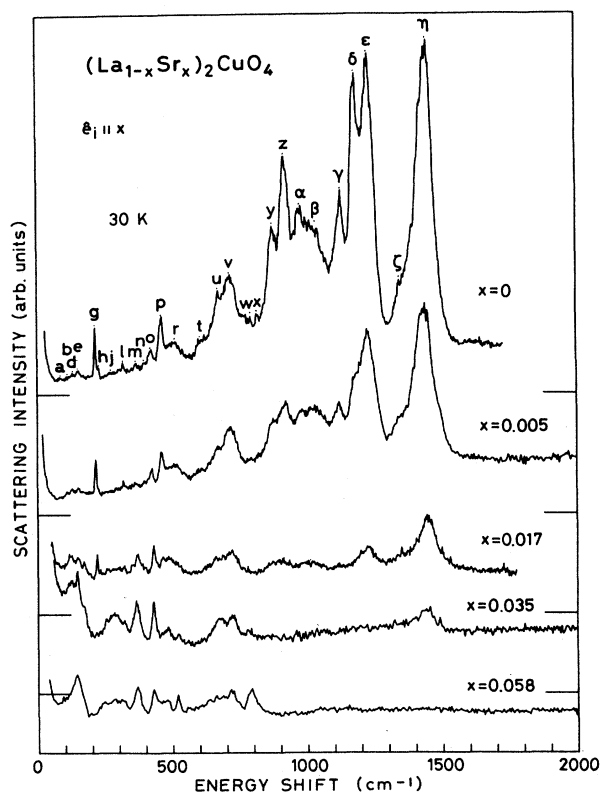


FIG. 3. Raman spectra of $(\text{La}_{1-x}\text{Sr}_x)_2\text{CuO}_4$ with $x=0, 0.005, 0.017, 0.035$, and 0.058 in the $(x+z, z)$ polarization configuration.

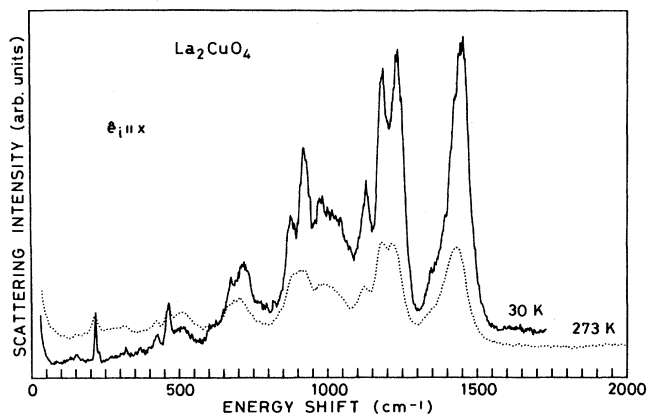


FIG. 4. Raman spectra of La_2CuO_4 at 30 and 273 K in the $(x, x+y)$ polarization configuration.

$x=0.015$. The 216 and 462 cm^{-1} peaks observed in La_2CuO_4 disappear at $x > 0.02$. In place of them broad peaks at $150, 283, 371 \text{ cm}^{-1}$ become strong. At high Sr concentration the 792 cm^{-1} peak becomes strong. The drastic change of the spectra by the small substitution cannot be explained, if no special electron-phonon interaction is present. The energies of the observed peaks are listed in Table II.

Figure 4 shows the temperature dependence of the

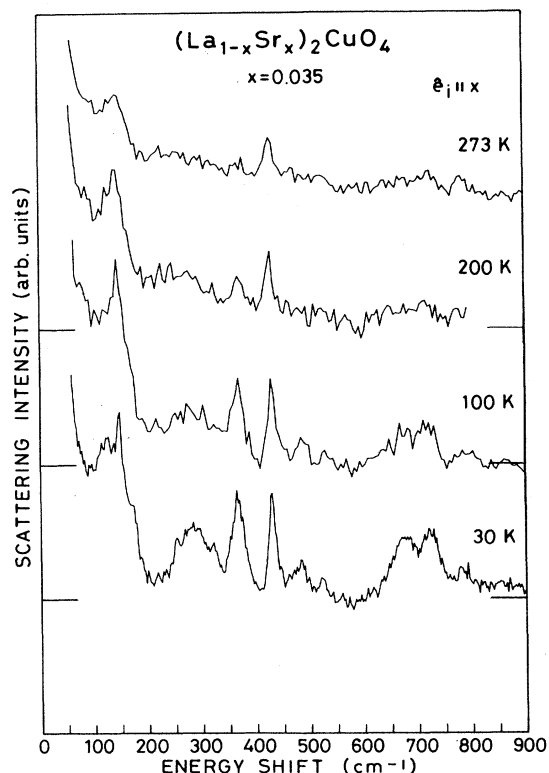


FIG. 5. Temperature dependence of the Raman spectra in the $(\text{La}_{1-x}\text{Sr}_x)_2\text{CuO}_4$ with $x=0.035$ in the $(x, x+y)$ polarization configuration.

TABLE II. Raman (R) and infrared (IR) active phonon energies (cm^{-1}) in $(\text{La}_{1-x}\text{Sr}_x)_2\text{CuO}_4$ at 30 K. Mode labels are the same as in Fig. 3. (s: strong, b: broad).

Mode	$x=0$			$x=0.005$		$x=0.017$		$x=0.035$			$x=0.058$	
	R ($x, x+y$)	R (z, z)	R (x, z)	R ($x, x+y$)	R ($x, x+y$)	R ($x, x+y$)	R ($x, x+y$)	R (z, z)	R (x, z)	IR $\hat{e} \parallel x$	IR $\hat{e} \parallel z$	R ($x, x+y$)
a	85			86								
b	112			111								
c		126s						108s				
d	132			129	122	124						
e	152	156s		152	150	147s	149			142		144sb
f					171	170						
g	216s		219	217s	220s							
h	227	229s		226		226	229s					
i					260	252			257		256	243
j	273	273s					273s					
k					283b	283sb						284sb
l	318			318	321	321						314
m	366			363	371s	365s			372	366		369s
n	398			398	399							
o	424s	426s		426s	431s	428s	430s					429s
p	462s			462s	465							
q					489b	484b						479b
r	511sb			513sb								
s						523	523s				510	519s
t	608			605								
u	673s			670sb	671b	677sb						670sb
v	716sb			714sb	722sb	723sb						718sb
w	792			790		782						792sb
x	818											
y (o+p)	876s			875s	898b							
z (2p)	919s			922s								
α (p+r)	976s			982s	1010b							
β (2r)	1023sb			1023s		1056						
γ (p+u)	1129s			1120s	1118							
δ (r+u, p+v)	1182s			1181s	1200							
ϵ (r+v)	1232s			1229s	1227s							
ζ (2u)	1347			1347	1349							
η (2v)	1449s			1436s	1446s	1438s						

($x, x+y$) Raman spectra in La_2CuO_4 . At high temperatures the intensities of the two-phonon peaks decrease markedly along with that of the two-magnon peak. It suggests that the intermediate electronic state of resonant scattering, which is related to the antiferromagnetic spin order, moves away from the resonant condition or broadens by the thermal fluctuation. The single-phonon peaks at 673 and 716 cm^{-1} also show large intensity decrease with the increase of the temperature. As discussed later these modes are forbidden in this polarization configuration. The large energy shift of the two-phonon peaks at 1232 and 1449 cm^{-1} (at 30 K) is due to the large temperature dependence of the peak energy of the 716 cm^{-1} (at 30 K) component mode.

Figure 5 shows the temperature dependence of the ($x, x+y$) spectra in $(\text{La}_{1-x}\text{Sr}_x)_2\text{CuO}_4$ with $x=0.035$. The orthorhombic-tetragonal transition temperature for this Sr concentration is about 300 K. On increasing temperature the intensities of most peaks decrease toward the structural transition temperature except for the 147 and

428 cm^{-1} (at 30 K) peaks. The 428 cm^{-1} mode is assigned to the A_g mode which is Raman active even in the tetragonal phase as discussed later in detail.

B. ($x+z, z$) spectra

Figure 6 shows the temperature dependent Raman spectra of $(\text{La}_{1-x}\text{Sr}_x)_2\text{CuO}_4$ in the ($x+z, z$) polarization configuration. The scattered light is not analyzed for the spectra shown in this figure, but it is checked that all the peaks except for the small 219 cm^{-1} peak have a polarization selection rule of (z, z), that is the A_g symmetry. The 219 cm^{-1} peak has a polarization selection of (x, z) which is for the B_{2g} or B_{3g} mode. All the peaks observed in the (z, z) polarization are also observed in the (x, x) spectra as expected from the selection rule except for the soft mode at the lowest energy. In the ($x+z, z$) polarization configuration the two-phonon scattering peaks are very weak. The spectra below 273 K are obtained in He

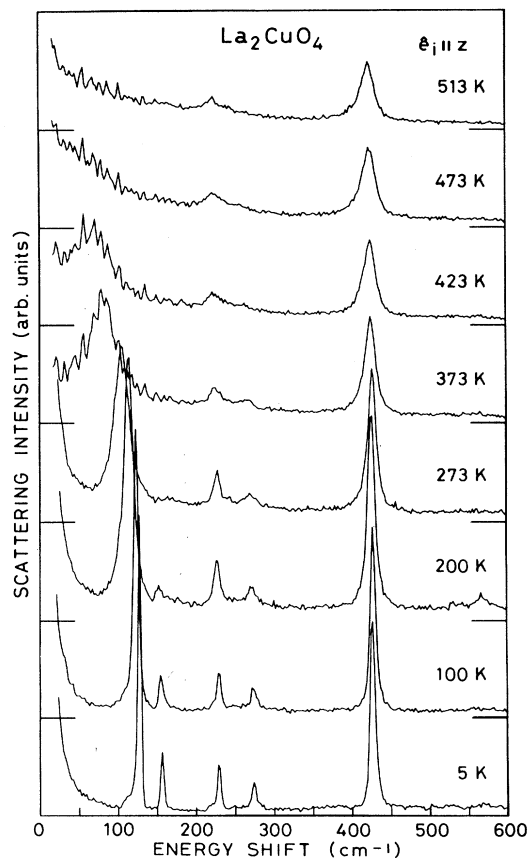


FIG. 6. Temperature-dependent Raman spectra of La_2CuO_4 in the $(x+z, z)$ polarization configuration.

gas, while those above it in air. The spectra measured in air are noisy because of the superposition of the Raman signal from air besides the sample. All the five A_g peaks expected from the normal-mode analysis are observed at 126, 156, 229, 273, and 426 cm^{-1} at 5 K. The 126 cm^{-1} mode is assigned to the staggered rotational mode of CuO_6 octahedra shown in Fig. 2(a). This mode shows softening toward the orthorhombic-tetragonal phase-transition temperature at 515 K. This mode becomes overdamped above 473 K. The energy is much higher than that of the soft mode observed by neutron scattering.²⁹ The observed peak energies are listed in Table II.

Figure 7(a) shows the temperature dependence of the energy of the 126 cm^{-1} (at 5 K) mode. The energy is determined by fitting the spectra with Gaussian curves after dividing the measured spectra by the statistical factor $n+1$ for the Stokes side. Here n is the Bose factor. Above 470 K this mode becomes an overdamped mode. At high temperatures the energy shifts upward as it is seen in the figure, but this is only caused by the correction process in which the flat background spectra composed of the luminescence and the stray light are divided by the statistical factor.

The temperature dependence of the peak intensity and the width expressed by the mean-square error σ of the fitted Gaussian curve is plotted in Figs. 7(b) and 7(c), re-

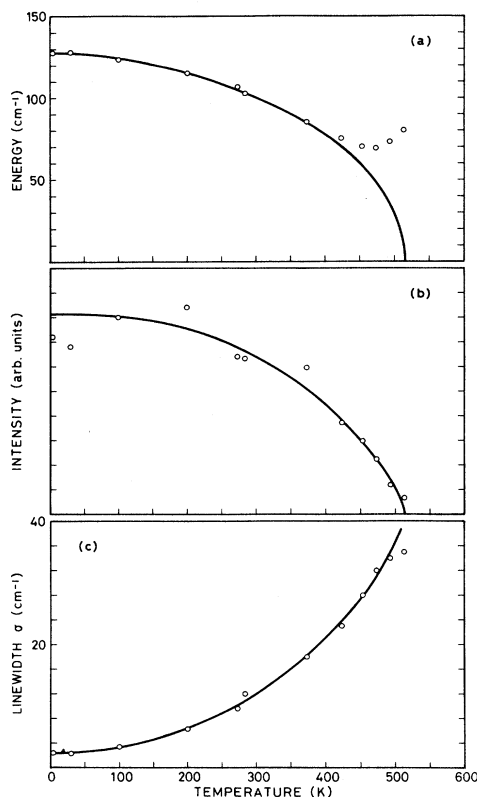


FIG. 7. (a) Energy, (b) the intensity, and (c) the width expressed by the mean-square error of the fitted Gaussian curve for the soft mode as a function of temperature. These physical quantities are obtained by fitting the spectra with Gaussian curves after dividing the measured spectra by the statistical factor $n+1$.

spectively. On approaching the orthorhombic-tetragonal phase-transition temperature at 515 K the intensity approaches zero and the linewidth increases as in a second-order phase transition.

Figure 8 shows the temperature dependent Raman spectra of $(\text{La}_{1-x}\text{Sr}_x)_2\text{CuO}_4$ with $x=0.035$ in the $(x+z, z)$ polarization. The soft mode related to the structural phase transition is observed at 108 cm^{-1} (at 30 K). The energy approaches zero at a lower temperature than in La_2CuO_4 .

Figure 9 shows the polarized Raman spectra of (z, z) and (x, z) configurations at 30 and 337 K. The atmosphere around the sample is He for the measurements at both temperatures. In the (z, z) configuration $5A_g$ modes are active in the orthorhombic phase and $2A_{1g}$ modes in the tetragonal phase. In (x, z) the $6B_{2g}+4B_{3g}$ modes are active in the orthorhombic phase and the $2E_g$ modes in the tetragonal phase. The sample is orthorhombic at 30 K and tetragonal at 337 K. The peak energies in the (z, z) spectra are 108, 149, 229, 273, 430, and 523 cm^{-1} at 30 K and 229, 433, and 525 cm^{-1} at 337 K. The energies in the (x, z) spectra are 229, 257, 372, and 429 cm^{-1} at 30 K and 237 cm^{-1} at 337 K. The appearance of the 523 cm^{-1} peak which is absent in La_2CuO_4 gives a larger

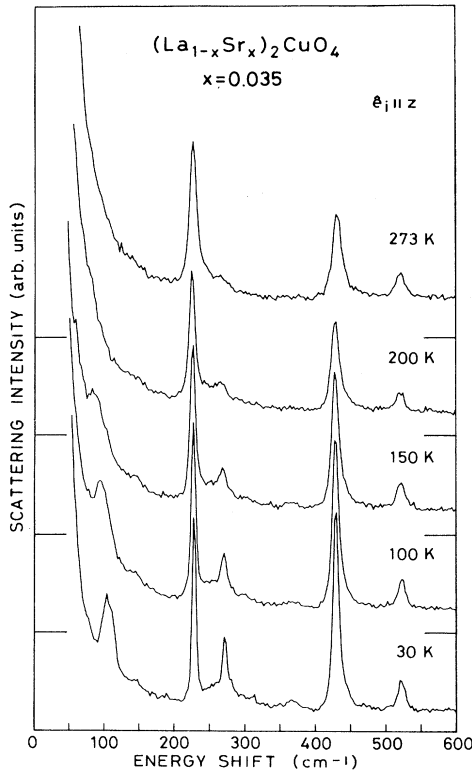


FIG. 8. Temperature dependence of the Raman spectra of $(\text{La}_{1-x}\text{Sr}_x)_2\text{CuO}_4$ with $x=0.035$ in the $(x+z, z)$ polarization configuration.

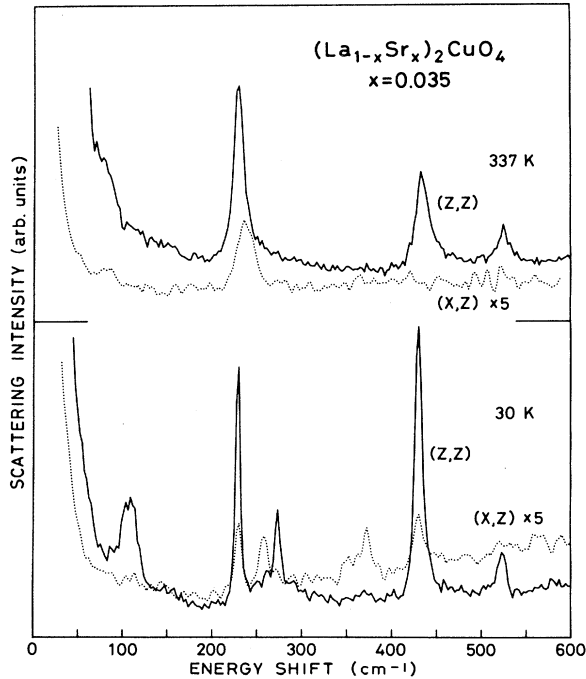


FIG. 9. Raman spectra of $(\text{La}_{1-x}\text{Sr}_x)_2\text{CuO}_4$ with $x=0.035$ at 30 and 337 K in the (z, z) (solid curves) and (x, z) (dotted curves) polarization configurations.

number of the A_g modes than expected from the group theoretical analysis in the orthorhombic structure. The appearance of the same peaks in both (z, z) and (x, z) spectra at 30 K also suggests that the crystal is of lower symmetry than orthorhombic. Details are discussed later.

The observed Raman peak energies at 30 K are summarized in Table II. The peaks observed in the $(x+z, z)$ spectra also appear in the $(x, x+y)$ spectra except for the soft-phonon peak with the lowest energy. The 273 cm^{-1} peak in the $(x+z, z)$ spectra of the $x=0.035$ is included in the broad peak at 283 cm^{-1} in the $(x, x+y)$ spectra. Table II lists also the infrared active transverse optical-phonon energies obtained from the Kramers-Kronig transformation from the reflection spectra on the same single crystal of $(\text{La}_{1-x}\text{Sr}_x)_2\text{CuO}_4$ with $x=0.035$. In the infrared spectra with the light polarized parallel to the layer the B_{2u} and B_{3u} modes are observed and the B_{1u} modes are observed with the light perpendicular to the layer.

C. Resonant Raman scattering

The strong scattering intensity of the two-phonon peaks at small x in $(\text{La}_{1-x}\text{Sr}_x)_2\text{CuO}_4$ is due to the resonant effect. Figure 10 shows the Raman spectra taken with various excitation wavelengths. Upon increasing the incident phonon energy by changing the laser wavelengths from 5145, 4880, to 4579 Å the two-phonon peaks de-

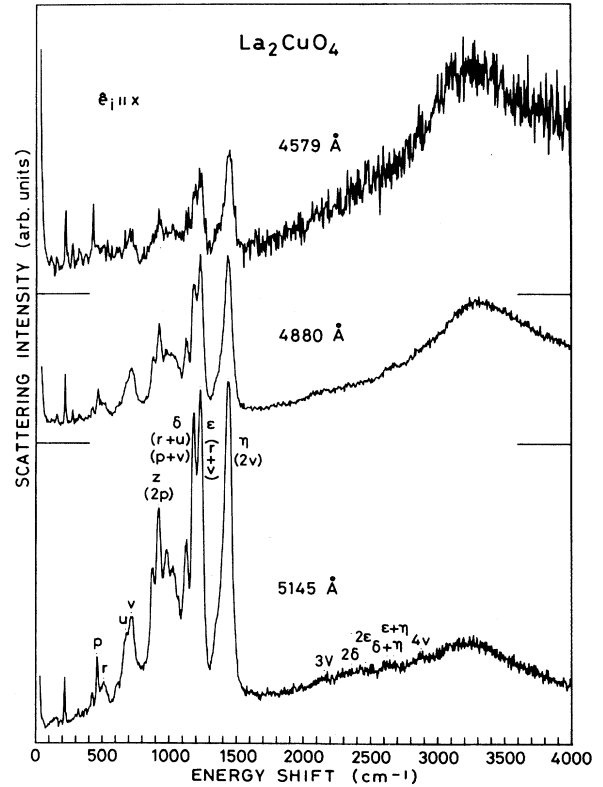


FIG. 10. Incident wavelength dependence of the Raman spectra in La_2CuO_4 at 30 K.

crease in intensity, while that of the two-magnon peak at about 3200 cm^{-1} increases.²⁰ The enhancement of the higher energy peak with the increase of the incident photon energy suggests that the system is under the out-going resonant condition. The estimated transition energy between the intermediate electronic states is about 18000 cm^{-1} (2.2 eV) with a very short width of about 1000 cm^{-1} . This energy width is too narrow to assign the states to the normal bands. These electronic levels are probably localized levels related with the Cu spin order, because the resonant effect disappears simultaneously with the extinction of the two-magnon peak on increasing Sr concentration.

V. MODE ASSIGNMENT

One of the characteristics of the Raman scattering in $(\text{La}_{1-x}\text{Sr}_x)_2\text{CuO}_4$ is the difference in the spectra of the $(x, x+y)$ and $(x+z, z)$ polarization configurations. The spectra in $(x+z, z)$ show normal-phonon scattering behavior, while the $(x, x+y)$ spectra are very complicated by the superposition of scattering from free carriers, magnons and multiphonons, and their coupling. Even in the single-phonon scattering the number of peaks are much larger than expected from the selection rules. This is interpreted as meaning that the Raman inactive phonon modes for the $(x, x+y)$ polarization appear in the spectra by the modification of the symmetry due to the interaction with the magnon or free carriers which are active in the (x, x) polarization. The number of peaks, 5, appearing in the (z, z) polarization spectra of Fig. 6 is the same as the number of the A_g modes in the orthorhombic phase. The lowest energy mode of 126 cm^{-1} (at 5 K) is the rotational mode of CuO_6 octahedra shown in Fig. 2(a). This mode is related with the orthorhombic distortion as discussed above. The 229 and 426 cm^{-1} peaks are observed even in the tetragonal phase, so that the 229 cm^{-1} mode is assigned to the vibration of La atoms along the z axis as listed in Table I, and the 426 cm^{-1} mode to the axial breathing mode as shown in Fig. 2(c). The 156 cm^{-1} mode is assigned to the vibration of the La atoms along the x axis as listed in Table I, and the 273 cm^{-1} mode to the mode shown in Fig. 2(b).

Most of the two-phonon peak energies are decomposed into sums of Raman active mode energies of p (462 cm^{-1} at $x=0$), r (511 cm^{-1}), u (673 cm^{-1}), and v (716 cm^{-1}) as listed in Table I. Usually two-phonon spectra indicate the phonon density of states because the simultaneous scattering of k and $-k$ phonons makes the two-phonon spectra. While only $k \sim 0$ phonon appear in the single-phonon spectra from the momentum conservation. However, if some phonons have very strong electron-phonon interaction, the combination of those modes appear dominantly in the spectra. So the p , r , u , and v modes are the specific modes with very strong electron-phonon interaction. In these compounds the mode which modifies the in-plane Cu—O bond length has large electron-phonon interaction. Two kinds of B_{2g} planar breathing modes shown in Figs. 2(d) and 2(e) and two kinds of B_{3g} planar quadratic modes shown in Figs. 2(f) and 2(g) are the relevant modes. In the tetragonal phase these modes are

the zone-boundary modes and are Raman inactive, while in the orthorhombic phase they become Γ -point modes. The B_{2g} modes are active in (a, c) and the B_{3g} modes in (b, c) , so that they are forbidden in the $(x, x+y)$ spectra. But it seems reasonable to assign the 673 , 716 , 462 , and 511 cm^{-1} modes in the $(x, x+y)$ spectra to the B_{2g} planar breathing modes shown in Figs. 2(d) and 2(e), and the B_{3g} planar quadratic modes of Figs. 2(f) and 2(g), respectively, for the following reasons: First, the $(x, x+y)$ spectra show a much larger number of peaks than eight expected from group theory. The extra peaks should have forbidden symmetry in themselves. Second, these modes are expected to have the highest four energies of the normal modes with large scattering intensities. Third, it is expected that the coupling of phonon with magnetic excitations or free carriers modifies the phonon symmetry, especially at resonance. The fact that the two-phonon peaks have larger intensities than the single-phonon peaks is probably related to the forbidden selection rule of those modes for single-phonon scattering in this polarization configuration. Those modes are not observed in the $(z, x+y)$ spectra in which they are allowed. Those modes are enhanced by the electronic transition which enhances the polarizability within the Cu—O plane.

VI. DISCUSSION

The Raman spectra of $(\text{La}_{1-x}\text{Sr}_x)_2\text{CuO}_4$ are anomalous compared with other compounds with orthorhombic structure. The Raman spectra are different from the polycrystalline Sr_2TiO_4 which is isostructural with tetragonal $(\text{La}_{1-x}\text{Sr}_x)_2\text{CuO}_4$.³⁷ The phonon energies used in the calculation of lattice dynamics^{38,39} are not in agreement with the present Raman data. The spectra in the $(x, x+y)$ and $(x+z, z)$ polarization configuration are very different. The $(x+z, z)$ spectra in La_2CuO_4 seem to satisfy the Raman selection rule for the orthorhombic structure, but the $(x, x+y)$ spectra include many peaks which are forbidden in this polarization. This is supposed to be due to the interaction of phonons with magnons or free carriers.

In the case of $(\text{La}_{1-x}\text{Sr}_x)_2\text{CuO}_4$ with $x=0.035$ even in the $(x+z, z)$ polarization configuration the spectra include more peaks than expected in the orthorhombic structure. The 523 cm^{-1} peak which is absent in La_2CuO_4 remains even in the so-called tetragonal phase at 337 K in the (z, z) spectra. If defects in a crystal increase by the substitution of Sr for La, it is possible that the forbidden modes appear in the spectra by the break of the symmetry. It is, however, unusual that the substitution of only a few percent of atoms causes the appearance of a new Raman peak with almost the same intensity as originally Raman active modes. The crystal is supposed to be of lower symmetry structure. In the (z, z) spectra only A_g modes are allowed, so the crystal structure is speculated to be monoclinic. The existence of the monoclinic structure at low temperatures is pointed out by high-resolution x-ray diffraction in $(\text{La}_{0.9}\text{Ba}_{0.1})_2\text{CuO}_{4-\delta}$ below 150 K (Ref. 40) and $(\text{La}_{0.925}\text{Sr}_{0.075})_2\text{CuO}_4$ below 220 K .⁴¹ For the latter case a triclinic distortion is also pointed out below 145 K .⁴¹ The (z, z) Raman spectra in-

dicates the tetragonal phase at $x=0.035$ is different from the K_2NiO_4 structure. Some atomic distortion remains above 300 K. In the $(x, x+y)$ spectra the 147 and 365 cm^{-1} peaks which are near the dominant infrared B_{2u} or B_{3u} mode energies of 142 and 366 cm^{-1} are enhanced and the strong peaks at 283 and 523 cm^{-1} appear a little above the B_{1u} mode energies of 256 and 510 cm^{-1} . The infrared and Raman activity is exclusive for the crystal with inversion symmetry. If the appearance of the infrared mode in the Raman spectra is due to the loss of the inversion symmetry, the energies should be the same. In this case the appearance of the infrared modes at slightly different energies may be due to some specific electronic transition coupled with the infrared modes makes them Raman active. It is contrary to the case of $BaBiO_3$ in which charge transfer coupled with the antiphase breathing mode in dimerized BiO_6 octahedra makes the breathing-type Raman mode active in the infrared spectra.⁴²

The correlation length of the two-dimensional antiferromagnetic spin order decreases rapidly on increasing the Sr concentration. The rapid decrease of the correlation length is related with the origin of the rapid decrease of the three-dimensional T_N . The antiferromagnetic spin order is related with the electronic levels with the transition energy of 2.2 eV which causes the resonant Raman scattering for the visible light. This electronic state disappears rapidly with the increase of x . The resonant two-phonon scattering is distinguished from the common resonant multiphonon scattering in which multiphonon peaks decrease with the increase of the order as in the case of $BaBiO_3$.⁴² It is noteworthy that in the case of $(La_{1-x}Sr_x)_2CuO_4$ the intensity of the two-phonon peak is larger than the single-phonon peak, but the three- and four-phonon peaks decrease abruptly. The boundary energy 1500 cm^{-1} for enhancement and suppression of the multiphonon peaks is just half of the two-magnon peak energy. It is speculated that there is an excitation band below 1500 cm^{-1} which is related with the antiferromagnetic spin order and the interaction with multiphonons makes the strong two-phonon peaks. The strong interac-

tion between phonons and magnons suggests that the complex state composed of phonons and magnons can contribute to form hole pairs of the superconductivity.

In the case of $BaBiO_3$ the multiphonon peaks of the 560 cm^{-1} breathing mode are observed up to the fifth order.⁴² In $YBa_2Cu_3O_{7-\delta}$ only a small two-phonon peak is observed despite the fact that the system is in the resonant condition. In the simple picture it is suggested from the number of higher harmonic peaks that the electron-phonon interaction decreases in order from $BaPb_{1-x}Bi_xO_3$, $(La_{1-x}Sr_x)_2CuO_4$ to $YBa_2Cu_3O_{7-\delta}$ as is the order of the magnitude of the isotope effect.

VII. CONCLUSIONS

To conclude, we remark the relation between the change in the phonon Raman spectra and the magnetic properties in $(La_{1-x}Sr_x)_2CuO_4$ with the increase of Sr concentration. On increasing Sr concentration, the resonant two-phonon peaks disappear simultaneously with the two-magnon peak. This change is related with the decrease of the correlation length of the two-dimensional antiferromagnetic spin order. The spectra of $(x, x+y)$ and $(x+z, z)$ are very different. The $(x, x+y)$ spectra show rich structure which is speculated to be caused by the phonon-magnon or phonon-free carrier interaction. In the $(x+z, z)$ spectra the soft-mode related to the orthorhombic-tetragonal phase transition is observed. The energy of this mode is much higher than that observed by the neutron scattering. The $(x+z, z)$ spectra indicate that the crystal symmetry is lower than orthorhombic for $x > 0.01$.

ACKNOWLEDGMENTS

The author would like to thank S. Shamoto and M. Sato for providing good single crystals. This work was supported by the Grant-in-Aid for Scientific Research on Priority Areas "Mechanism of Superconductivity" from the Ministry of Education, Science, and Culture of Japan.

¹J. G. Bednorz and K. A. Müller, Z. Phys. B **64**, 189 (1986).

²W. Weber, Phys. Rev. Lett. **58**, 1371 (1987).

³H. Fukuyama and Y. Hasegawa, J. Phys. Soc. Jpn. **56**, 1312 (1987).

⁴C. L. Fu and A. J. Freeman, Phys. Rev. B **35**, 8861 (1987).

⁵T. A. Falten, W. K. Ham, S. W. Keller, K. J. Leary, J. N. Michaels, A. M. Stacy, H.-C. zur Loye, D. E. Morris, T. W. Barbee III, L. C. Bourne, M. L. Cohen, S. Hoen, and A. Zettl, Phys. Rev. Lett. **59**, 915 (1987).

⁶B. Batlogg, R. J. Cava, A. Jayaraman, R. B. van Dover, G. A. Kourouklis, S. Sunshine, D. W. Murphy, L. W. Rupp, H. S. Chen, A. White, K. T. Short, A. M. Mjssce, and E. A. Rietman, Phys. Rev. Lett. **58**, 2333 (1987).

⁷L. C. Bourne, M. F. Crommie, A. Zettl, H.-C. zur Loye, S. W. Keller, K. L. Leary, A. M. Stacy, K. J. Chang, M. L. Cohen, and D. E. Morris, Phys. Rev. Lett. **58**, 2337 (1987).

⁸B. Batlogg, G. Kourouklis, W. Weber, R. J. Cava, A. Jayaraman, A. E. White, K. T. Short, L. W. Rupp, and E. A. Riet-

man, Phys. Rev. Lett. **59**, 912 (1987).

⁹L. C. Bourne, A. Zettl, T. W. Barbee III, and M. L. Cohen, Phys. Rev. B **36**, 3990 (1987).

¹⁰K. J. Leary, H.-C. zur Loye, S. W. Keller, T. A. Falten, W. K. Ham, J. N. Michaels, and A. M. Stacy, Phys. Rev. Lett. **59**, 1236 (1987).

¹¹H. Katayama-Yoshida, T. Hirooka, A. J. Mascarenhas, Y. Okabe, T. Takahashi, T. Sasaki, A. Ochiai, T. Suzuki, J. I. Pankove, T. Cizek, and S. K. Deb, Jpn. J. Appl. Phys. **26**, L2085 (1987).

¹²D. Vaknin, S. K. Sinha, D. E. Moncton, D. C. Johnston, J. W. Newsam, C. R. Safinya, and H. E. King, Jr., Phys. Rev. Lett. **58**, 2802 (1987).

¹³S. Mitsuda, G. Shirane, S. K. Sinha, D. C. Johnston, M. S. Alvarez, D. Vaknin, and D. E. Moncton, Phys. Rev. B **36**, 822 (1987).

¹⁴T. Freltoft, J. E. Fisher, G. Shirane, D. E. Moncton, S. K. Sinha, D. Vaknin, J. P. Remeika, A. S. Cooper, and D.

- Harshman, Phys. Rev. B **36**, 826 (1987).
- ¹⁵Y. J. Uemura, W. J. Kossler, X. H. Yu, J. R. Kempton, H. E. Schone, D. Opie, C. E. Stronach, D. C. Johnston, M. S. Alvarez, and D. P. Goshorn, Phys. Rev. Lett. **59**, 1045 (1987).
- ¹⁶D. C. Johnston, J. P. Stokes, D. P. Goshorn, and J. T. Lewandowski, Phys. Rev. B **36**, 4007 (1987).
- ¹⁷G. Shirane, Y. Endoh, R. J. Birgeneau, M. A. Kastner, Y. Hidaka, M. Oda, M. Suzuki, and T. Murakami, Phys. Rev. Lett. **59**, 1613 (1987).
- ¹⁸K. B. Lyons, P. A. Fleury, J. P. Remeika, A. S. Cooper, and T. J. Negran, Phys. Rev. B **37**, 2353 (1988).
- ¹⁹Y. Kitaoka, K. Ishida, S. Hiramatsu, and K. Asayama, J. Phys. Soc. Jpn. **57**, 734 (1988).
- ²⁰S. Sugai, S. Shamoto, and M. Sato, Phys. Rev. B **38**, 6463 (1988).
- ²¹N. Nishida, H. Miyatake, D. Shimada, S. Okuma, M. Ishikawa, T. Takabatake, Y. Nakazawa, Y. Kuno, R. Keitel, J. H. Brewer, T. M. Riseman, D. L. Williams, Y. Watanabe, T. Yamazaki, K. Nishiyama, K. Nagamine, E. J. Ansaldo, and E. Torikai, Jpn. J. Appl. Phys. **26**, L1856 (1987).
- ²²J. M. Tranquada, D. E. Cox, W. Kunmann, H. Moudden, G. Shirane, M. Suenaga, P. Zolliker, D. Vaknin, S. K. Sinha, M. S. Alvarez, A. J. Jacobson, and D. C. Johnston, Phys. Rev. Lett. **60**, 156 (1988).
- ²³Y. Kitaoka, S. Hiramatsu, K. Ishida, K. Asayama, H. Takagi, H. Iwabuchi, S. Uchida, and S. Tanaka, J. Phys. Soc. Jpn. **57**, 737 (1988).
- ²⁴S. Sugai, M. Sato, and S. Hosoya, Jpn. J. Appl. Phys. **26**, L495 (1987).
- ²⁵T. Brun, M. Grimsditch, K. E. Gray, R. Bhadra, V. Maroni, and C.-K. Loong, Phys. Rev. B **35**, 8837 (1987).
- ²⁶S. Blumenroeder, E. Zirngiebl, J. D. Thompson, P. Killough, J. L. Smith, and Z. Fisk, Phys. Rev. B **35**, 8840 (1987).
- ²⁷M. Čopič, D. Mihailović, M. Zgonik, M. Prester, K. Biljako-
vić, B. Orel, and N. Brničević, Solid State Commun. **64**, 297 (1987).
- ²⁸G. A. Kourouklis, A. Jayaraman, W. Weber, J. P. Remeika, G. P. Espinosa, A. S. Cooper, and R. G. Maines, Sr., Phys. Rev. B **36**, 7218 (1987).
- ²⁹R. J. Birgeneau, C. Y. Chen, D. R. Gabbe, H. P. Jenssen, M. A. Kastner, C. J. Peters, P. J. Picone, T. Thio, T. R. Thurston, H. L. Tuller, J. D. Axe, P. Böni, and G. Shirane, Phys. Rev. Lett. **59**, 1329 (1987).
- ³⁰Von B. Grande, Hk. Müller-Buschbaum, and M. Schweizer, Z. Anorg. Allg. Chem. **428**, 120 (1977).
- ³¹J. M. Longo and P. M. Raccach, J. Solid State Chem. **6**, 526 (1973).
- ³²H. Takagi, S. Uchida, K. Kitazawa, and S. Tanaka, Jpn. J. Appl. Phys. **26**, L123 (1987).
- ³³J. D. Jorgensen, H.-B. Schüttler, D. G. Hinks, D. W. Capone, II, K. Zhang, M. B. Brodsky, and D. J. Scalapino, Phys. Rev. Lett. **58**, 1024 (1987).
- ³⁴T. Fujita, Y. Aoki, Y. Maeno, J. Sakurai, H. Fukuba, and H. Fujii, Jpn. J. Appl. Phys. **26**, L368 (1987).
- ³⁵R. J. Cava, A. Santoro, D. W. Johnson, Jr., and W. W. Rhodes, Phys. Rev. B **35**, 6716 (1987).
- ³⁶R. M. Fleming, B. Batlogg, R. J. Cava, and E. A. Rietman, Phys. Rev. B **35**, 7191 (1987).
- ³⁷G. Burns, F. H. Dacol, and M. W. Shafer, Solid State Commun. **62**, 687 (1987).
- ³⁸J. Prade, A. D. Kulkarni, F. W. de Wette, W. Kress, M. Cardona, R. Reiger, and U. Schröder, Solid State Commun. **64**, 1267 (1987).
- ³⁹S. Mase, T. Yasuda, Y. Horie, and T. Fukami, Solid State Commun. **65**, 477 (1988).
- ⁴⁰S. C. Moss, K. Forster, J. D. Axe, H. You, D. Hohlwein, D. E. Cox, P. H. Hor, R. L. Meng, and C. W. Chu, Phys. Rev. B **35**, 7195 (1987).
- ⁴¹K. Kamigaki, N. Sano, and H. Terauchi, Jpn. J. Appl. Phys. **26**, L1642 (1987).
- ⁴²S. Sugai, Phys. B **35**, 3621 (1987).